UAV-assisted RFET:
A Novel Framework for Sustainable WSN

Suraj Suman, Sidharth Kumar, and Swades De

Abstract—Limited battery capacity is one of the major hurdles towards perpetual operation of wireless sensor networks. In this paper, a novel framework for charging the sensor nodes using unmanned aerial vehicle (UAV)-assisted radio frequency energy transfer (RFET) is presented. First, the notion of RFET zone is conceptualized and a closed-form expression for RFET zone radius is obtained. The sensor nodes located inside this zone can harvest energy from the transmitter mounted on UAV. The effective power harvested at the sensor node situated at different spatial locations is evaluated by considering the impact of shadowing statistics of path loss and non-linear RF-to-direct current conversion efficiency. With these findings on sensor nodes deployed in a given area, an optimization problem is formulated with the objective of minimizing the total time in a charging cycle, which is comprised of travel time and charging time. This problem is decomposed into two sub-problems and they are solved individually in sequential steps. The optimal solution of the first sub-problem, which provides the sequence of charging having minimum travel time, is a Traveling Salesman Problem (TSP). In the second sub-problem, the presence of Lambert function makes it analytically intractable, and hence, approximations are presented to solve this. Subsequently, to account for the health parameters of the sensor nodes in estimating the charging cycle, three variants of order of charging, namely, *Voltage-aware Charging Sequence*, *Operational Time-aware Charging Sequence*, and *Iterative Charging Sequence*, are proposed. Through system simulations it is demonstrated that, in a generalized setting, the charging sequence offered by the proposed variants perform increasingly better in comparison to the state-of-the-art TSP approach.

Index Terms—Unmanned aerial vehicle, IoT, wireless sensor network, wireless power transfer, radio frequency energy transfer, traveling salesman problem, generalized voltage and operational time aware charging

I. INTRODUCTION

In the fifth generation wireless (5G) era, the entire physical phenomena around us, such as area monitoring, health care, environmental sensing, industrial, smart grid, and agriculture, are envisioned to be monitored using Internet of Things (IoT) by making use of wireless sensor nodes [2]. Efficient communication technology, cost-effective, small size, and low power consumption are some features that have enabled the wireless sensor networks (WSNs) to be an integral part of IoT [3]. The field deployed sensor nodes are generally powered by batteries having finite lifetime and require periodic energy replenishment to avoid unwanted outage in network coverage and connectivity. Battery replacement is neither cost-effective nor feasible in many applications, such as in structural monitoring and pollution or hazardous chemical sensing, where sensor nodes are deployed in inaccessible locations. Moreover, the use of replaceable batteries is not environmentally friendly. As the number of IoT devices are expected to grow at a compound annual rate of 21% by the year 2022 [4], cost-effective energy replenishment for sustainable WSN operation in large-scale implementation is of major interest in the research community.

A. Related Work

Various methods have been reported aiming at maximizing the overall network lifetime. These approaches involve the design of efficient multi-access control [5] and routing protocols [6], with a combined objective of reducing energy footprint of the network and the individual nodes. In a network with static deployment, the nodes near the base station are more energy constrained, as they have to relay the data packets of other faraway nodes. This is a major drawback, as it creates avoidable energy holes in the network, causing network outage.

Treating mobility as boon, the concept of mobile base station was proposed to prolong the lifetime of sensor networks. The concept of a moving vehicle, called data MULE (Mobile ubiquitous LAN extension), was introduced in [7] to collect data by visiting different nodes in a deployment area. The main advantage of this method is that, the data sink can move to different locations to collect field data from sensor nodes as and when required, thus alleviating the problem of energy hole. The authors in [8] extended the idea of mobility to data relays, and the authors in [9] considered the scenario of multiple mobile data sink nodes. All these methods help to an extent to increase the network lifetime, but the issue of recharging the depleted batteries was not addressed.

To overcome the battery replacement issue, energy harvesting from several ambient sources, such as solar, vibration, piezoelectric, and ambient RF [10], [11], were proposed. Random nature of these sources and large dimension of deployed energy harvesting setup are the major hurdles towards usage of these approaches for sustainable WSN [12]. Moreover, the sensor nodes deployed in inaccessible locations may not be able to use these ambient sources. Therefore in order to ensure uninterrupted network operation, dedicated energy source is required for battery energy replenishment. Recently, wireless power transfer has been found to be a promising solution. This process is especially useful when it is difficult or infeasible to replace battery physically or recharge the node by connecting to an electrical outlet. Two well-known methods for this are non-radiative and radiative wireless power transfer [13].

Non-radiative wireless charging is based on coupling of magnetic field between coils of transmitter and receiver. Inductive coupling and magnetic resonance coupling are two prominent techniques for non-radiative power transfer. However, inductive coupling based energy transfer is not suitable for real-life deployment due to its very short communication range. On the other hand, magnetic resonance coupling has good power transfer efficiency over very short range; it degrades severely with distance. In contrast, radiative power transfer offers more flexibility on alignment and offers the advantage of beam steering. Also, the effect of interference due to transmission from multiple RF sources could aid in increased harvested energy [14].

Wireless power transfer based techniques, where mobile vehicle is used to charge the sensor nodes, have received significant attention [15]–[22]. In [15], [16], a dedicated mobile wireless charging vehicle (WCV) employing magnetic resonance coupling is used to charge the sensor nodes periodically with an objective to minimize the total time of WCV movement. Joint data gathering and magnetic resonance coupling based wireless charging using a mobile vehicle, called SenCar was reported in [17]. In magnetic resonance coupling based charging approaches, mobile vehicles have to reach very close to the field node to execute wireless power transfer [23], which is not always practically feasible in real life deployment scenario. Also, the information transfer and power transfer are done at different frequency bands, which require additional hardware. UAV based magnetic resonant power transfer was demonstrated to recharge the batteries of ground sensor nodes [18]. It was observed that, inexact positioning of coils, relative motion of coils due to vibration, and deformations in these coils degrade the performance severely.

Radio frequency energy transfer (RFET), which is electromagnetic radiation based, has also been explored towards sustainable network operation. Off-the-shelf devices, such as Powercast energy harvester [24] can be easily embedded in the sensor nodes to facilitate RFET. In [19], the concept of integrated data and energy mule (IDEM) was introduced, where advantage of multihop RFET was demonstrated leading to significant gains in energy and time. Similar works are reported in [21] and [22], where charging process and path planning problem were investigated. Safe charging for wireless power transfer is considered in [25], where static chargers are installed to maintain the power coverage. It requires the infrastructure establishment and power supply provisioning for these fixed static chargers, which is expensive. Also, such kind of arrangement can only be availed in well-furnished environment. The energy provisioning to battery-less wireless identification and sensing platform (WISP) is reported in [26].

Recently, UAV-enabled wireless power transfer has been reported in [27], where received energy at field node is optimized. However, the important aspects of non-linear rectification efficiency of power harvester and remaining battery energy of the sensor node have not been considered. On the other hand, the authors in [1] have evaluated the time required for charging the sensor nodes.

B. Motivation and Contribution

Previously reported powering approaches, such as WCV [15], SenCar [17], IDEM [19], where ground mobile vehicles are used, are constrained by physical as well technical difficulties. These ground based mobile vehicles can operate with suitable-furnished platform, such as in laboratory environments. In real-life deployment scenarios, such as in agricultural and forest environments, or in any other terrain with structural constraints, wireless charging using mobile ground vehicles may be severely constrained by physical path availability and reachability to the sensor nodes.

Now-a-days, UAVs are used for various applications, namely, logistics, medical emergency, agriculture, disaster management, and cellular architecture along with the traditional applications, such as surveying and monitoring, and defense [28], [29], [30]. The advancements in aircraft technology [31] enable UAVs to be useful in various applications, where autonomous flight can be scheduled to complete the task by establishing global positioning system (GPS) way-points on computer. Machine learning and artificial intelligence are expected to enable safe and stable trajectory accomplishment at very low altitude [32]. Motivated by the challenges associated with terrain mobility and the flexibility of RF radiation based charging, in this work a UAV-assisted RFET framework is presented for online charging of the field nodes. We argue that, UAV has the capability to overcome mobility bottlenecks for energy replenishment in diverse deployment scenarios.

In this paper, we present a UAV application for RFET based charging of wireless sensor nodes for IoT applications. In UAV-assisted RFET, RF transmitter is mounted on UAV, and path planning can be automated, as suggested by the proposed algorithm. Rotary-wing UAV is considered due to its capability of static hovering at an altitude for sufficient duration. Moreover, due to sufficient beam-width of RF radiation, vibration has much negligible impact on UAV-assisted RFET. RFET can provide on demand energy supply without additional radio hardware, as the energy as well as information transfer can be done over the same antenna, unlike magnetic resonance coupling. In this work, we restrict our discussion to energy replenishment, only because the receiver sensitivities are more stringent for energy transfer as compared to information transfer. Our preliminary studies have been recently reported in [1].

The work presented here distinguishes itself from the study in [27] in the sense that, in [27] the authors looked into the problem from transmitter perspective only, whereas in our work we investigate the energy replenishment and charging mechanism in order to optimize the overall system design from a joint viewpoint of transmitter and receiver. To this end, in this work we aim at accurately estimating the time required for online recharging the sensor nodes where (i) the non-linearity of rectification efficiency as a function of received RF power, (ii) initial battery energy dependent growth of energy level with time for a given received RF power, as well as (iii) charging and discharging impairments of supercapacitor are accounted. Free-space path-loss model was considered for analyzing the received power in [27], whereas in [1] path-loss model originally designed for cellular application (i.e.

from high altitude platform [33]) has been used. As shown in [34], for air-to-ground communication, free-space path loss model does not accurately estimate the receive power. Further, a recent study in [34] has shown that, for short transmitter-receiver distance, as in our considered RFET scenario, the model in [33] also gives an inaccurate estimate. Therefore, in contrast to the path-loss model considered in [27], in our analysis we consider the developed parametric path-loss model in [34] for UAV-assisted RFET.

The major contributions of this work are as follows:

1) A novel notion of RFET zone is conceptualized; all the sensor nodes within this zone can harvest energy from UAV. Net power harvested to the field nodes situated at different locations is obtained, which depends on path loss, shadow statistics, and RF-to-direct current (RF-to-DC) conversion efficiency.

2) When a sensor node is charged, other sensor nodes lying in the RFET zone also receive power, which leads to multi-sensor charging scenario at a time. According to this fact, optimization problem for a given number of nodes is formulated to minimize the total time of charging, which comprises of charging time of nodes and travel time. This problem is decomposed into two sub-problems and they are solved sequentially.

3) In this basic optimization, the optimal solution of first sub-problem is obtained by solving traveling salesman problem (TSP), that provides the traveling sequence and travel time. The second sub-problem deals with the optimal charging time of a node. Presence of Lambert function in the equations of constant power charging and discharging for a supercapacitor makes the problem analytically intractable. To this end, an approximation of Lambert function is presented, which offers excellent goodness of fit.

4) The performance in terms of number of healthy sensor nodes, that can be attended, is evaluated. Three different charging schemes namely *Voltage-aware Charging Sequence*, *Operational Time-aware Charging Sequence*, and *Iterative Charging Sequence* have been proposed. These schemes consider the parameters of the sensor node rather than distance only. It is demonstrated that *ICS* offers the best performance against other charging schemes.

C. Paper Organization

The paper is organized as follows. In Section II, the system model for UAV-assisted RFET is presented and effective power harvested at sensor nodes is derived. The optimization problem to estimate the charging time in a charging cycle is analyzed in Section III. Performance evaluation with the proposed different charging mechanisms is discussed in Section IV. Section V contains the simulation results, followed by the concluding remarks and future direction in Section VI.

II. SYSTEM MODEL

The system model for UAV-assisted RFET is shown in Fig. 1. The deployed field sensor nodes in a given area are to be charged by an energy transmitter mounted on UAV. Each

Table I: List of major variables along with their descriptions

h	Deployment altitude of UAV-mounted RFET source
θ	Elevation angle made by UAV at sensor node
L_{fs}	Free space path loss
$\mathcal{X}$	Excess path loss
L	Total path loss comprises of L_{fs} and $\mathcal{X}$
μ	Mean of excess path loss
σ^2	Variance of excess path loss
P_{rx}	Received power at sensor node
P_{tx}	Transmitted power by UAV-mounted RFET source
P_o	Sensitivity of RF power harvester
$q_{\mathcal{H}}$	Probability of energy harvesting
$P_{\mathcal{H}}$	Harvested power
P_{sen}	Effective power harvested at sensor node
T	Time of operation of each sensor node
v_I	Initial voltage level of sensor node
v_F	Final voltage level of sensor after charging/discharging
v_{th}	Threshold voltage of supercapacitor
$\underline{p}^k$	Power exchange vector over time vector $\underline{t}$ for k^{th} sensor node
p_d	Drain power of sensor node
A	Total area of sensor deployment
N_S	Number of deployed sensor nodes in a given area A
$\mathcal{U}$	Velocity of UAV during traveling

sensor node is equipped with an RF harvester to collect DC energy from received RF waveform, and this harvested energy is stored in a supercapacitor embedded with the sensor node for further use. In this section, a framework for RFET aware positioning of UAV is developed and net power available at the field sensor nodes is evaluated.
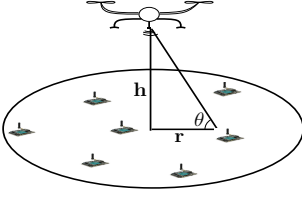
A. Path loss Model

The received power is a key parameter in RFET applications and it depends on the path loss faced by the RF signal. The path loss model dedicated for UAV-assisted RFET is reported in [34], which has been used here for analysis. The path loss $L(h, \theta)$ at a ground location, making an elevation angle θ with the power transmitter mounted on UAV hovering at height h as shown in Fig. 1 is given as:

$$L(h, \theta) = L_{fs}(h, \theta) + \mathcal{X}, \qquad (1)$$

where θ (in °) is elevation angle, $h \cdot \csc(\theta) = \sqrt{h^2 + r^2}$ is the separation distance between transmitter and receiver, and r is the horizontal distance of the node location from the ground projection point of the actual transmitter (cf. Fig. 1). $L_{fs}(h, \theta)$ is the free space path loss given as: $L_{fs}(h, \theta) = 20 \log_{10}(h \cdot \csc \theta) + 20 \log_{10}(f) - 10 \log_{10}(G_{tx}G_{rx}) + 32.44$. $\mathcal{X}$ is the elevation angle dependent excess path loss and given as: $\mathcal{X} \sim \mathcal{N}(\mu(\theta), \sigma^2(\theta))$, where $\mathcal{N}$ denotes the normal distribution having mean $\mu(\theta)$ and variance $\sigma^2(\theta)$. $\mu(\theta)$ and $\sigma^2(\theta)$ (both in dB) with $\mu(\theta) = a \cdot \exp(b \cdot \theta)$, $\sigma^2(\theta) = c \cdot \exp(d \cdot \theta)$. Suburban area is considered for analysis with $a = 12.05$, $b = -0.0742$, $c = 79.24$, and $d = -0.0817$.

Here, because RF transmission is done over a long time duration, up to a few minutes, the impact of small-scale fading

Figure 1: System model for UAV-assisted RFET.

is averaged out over such a long time period of operation. Accordingly, large-scale fading (i.e., shadowing) is accounted in the performance analysis. The path loss model expression in (1) incorporates the random fluctuation of received signal that arises over wireless channel due to reflection, diffraction, and scattering in terms of excess path loss along with the distance based free space path loss, where the excess path loss refers to shadowing [34].

B. Formation of RFET Zone

RFET works in the far-field region of an antenna generating (transmitting) electromagnetic waves, the power of signal reduces as the distance from transmitter is increased. The RF power harvester consists of a rectifying circuit, a voltage booster circuit, and a supercapacitor to store the harvested energy. The rectifying circuit is made up of low-pass filter followed by diode-based rectifier, which converts the incoming RF signal energy into DC power. The rectifier is able to harvest energy if the received power is above some threshold P_o, which is called RF energy harvesting sensitivity of the harvester. $P_o = -12$ dBm is considered in numerical results [24].

Definition 1. *RFET zone is the ground field area within which the sensor nodes are able to harvest energy from the RF wave transmitted from UAV while it hovers at a position.*

Definition 2. *The probability of energy transfer $q_{\mathcal{H}}(h, \theta)$ is the chance of an event for which the received power at a sensor node, making an elevation θ with UAV deployed at height h, is greater than the sensitivity of power harvester.*

The probability of energy transfer is defined to incorporate the random variation of received signal arises from real wireless channel occurring due to reflection, diffraction and scattering, which are being captured in excess path loss. The probability of energy transfer is obtained as:

$$q_{\mathcal{H}}(h, \theta) = \Pr\{P_{rx}(h, \theta) \geq P_o\}$$
$$= 1 - Q\left(\frac{P_{tx} - P_o - L_{fs}(h, \theta) - \mu(\theta)}{\sigma(\theta)}\right) \quad (2)$$

where $P_{rx}(h, \theta) = P_{tx} - L(h, \theta)$ is the received power at a location (h, θ). P_{rx} is also a Gaussian random variable with mean $P_{tx} - L_{fs}(h, \theta) - \mu(\theta)$ and variance $\sigma^2(\theta)$, as it is the linear transformed version of $\mathcal{X}$. $Q(\cdot)$ is the Gaussian Q-function defined as, $Q(x) = \int_x^\infty \frac{1}{\sqrt{2 \cdot \pi}} e^{\frac{-x^2}{2}} dx$.

The definition of RFET zone poses a limit on the maximum tolerable path loss in order to harvest energy from RF signal. Therefore, it is important to obtain the range of possible

heights of UAV deployment as well as the area of RFET zone. The RF transmission is done over a long time scale to charge the sensor nodes. Therefore, received power at a given location (h, θ) in expected sense is an appropriate choice rather than instantaneous sense while dimensioning the RFET zone. The expected value of received power corresponds to $q_{\mathcal{H}}(h, \theta) = 0.5$ due to Gaussian distribution of $P_{rx}(h, \theta)$.

The expected path loss $(\mathbb{E}[L(h, \theta)])$ is given as,

$$\mathbb{E}[L(h, \theta)] = L_{fs}(h, \theta) + \mu(\theta). \quad (3)$$

Lemma 1. *The expected value of path loss is not a convex function of height and radius.*

Proof. : See Appendix A. □

Lemma 2. *The expected value of path loss is a unimodal function of height for a given radius.*

Proof. : See Appendix B. □

Lemma 3. *The expected value of path loss is a non-decreasing function of radius for a given height.*

Proof. : See Appendix C. □

Remark 1. *For a node placed just below UAV, the radius is 0. Hence, a node located just below UAV will experience the minimum path loss due to non-decreasing nature of path loss with radius. Thus at this node, only height dependent path loss is present which can be obtained from (1) with $\theta = 90°$.*

The path loss model for UAV-assisted RFET is characterized in Lemmas 1, 2, and 3. It is observed that, the path loss is not a convex function of UAV coverage radius and deployment altitude. However, the path loss experiences unimodal variation against height for a given radius due to increase in free space path loss and decrease in excess path loss. As UAV deployment height increases, the effect of blockage caused by obstructions reduces, and hence excess path loss decreases. On the other hand, the path loss experiences non-decreasing variation against radius for a fixed deployment altitude of UAV, because the received signal faces more obstacles with increase in radius.

Now, if UAV is placed at a given height h_0, which is fixed but arbitrary, the radius of RFET zone or range of elevation angle can be obtained by solving the following equation:

$$\mathbb{E}[P_{rx}(h_0, \theta)] \leq P_o \Rightarrow \mathbb{E}[L(h_0, \theta)] \leq P_{tx} - P_o. \quad (4)$$

As the function is not convex (see Lemma 1), the radius for RFET zone can be obtained by solving $\mathbb{E}[L(h_0, \theta)] - P_{tx} + P_o = 0$ using numerical technique, like Bisection method [35] due to non decreasing nature of path loss (cf. Lemma 3). Since, it involves significant computation requirement, approximation technique is preferred. Using approximations, we obtain closed form expression of the radius of RFET zone. From (1) and (4),

$$20 \log_{10}(h_0 \cdot \csc(\theta)) + 20 \log_{10}(f)$$
$$- 10 \log_{10}(G_{tx}G_{rx}) + 32.44 + \mu(\theta) \leq P_{tx} - P_o \quad (5)$$

This equation involves logarithmic, trigonometric, and exponential functions, which are transcendental functions. Sin-

gularity of $\csc(\theta)$ at $\theta = 0$ is a major trouble and it is difficult to approximate these functions in finite sequence. Hence, we have approximated these functions using curve fitting technique in the range of $\theta \in [5°, 85°]$ to avoid singularity. $\log_{10}(\csc(\theta))$ is approximated as: $\log_{10}(\csc(\theta)) \approx \mathfrak{q}_3 \cdot \theta^3 + \mathfrak{q}_2 \cdot \theta^2 + \mathfrak{q}_1 \cdot \theta + \mathfrak{q}_o$, with $\mathfrak{q}_3 = -2.251 \times 10^{-5}, \mathfrak{q}_2 = 0.002161, \mathfrak{q}_1 = -0.08054, \mathfrak{q}_o = 1.385$ for $\theta \leq 40°$; $\mathfrak{q}_3 = -4.94 \times 10^{-7}, \mathfrak{q}_2 = 0.000181, \mathfrak{q}_1 = -0.02079, \mathfrak{q}_o = 0.7649$ for $40° < \theta \leq 85°$. The R-square value for this fitting is 0.9935, which indicates excellent fitting. $\exp(b \cdot \theta)$ is approximated as: $\exp(b \cdot \theta) \approx \mathfrak{p}_3 \cdot \theta^3 + \mathfrak{p}_2 \cdot \theta^2 + \mathfrak{p}_1 \cdot \theta + \mathfrak{p}_o$, with $\mathfrak{p}_3 = -1.414 \times 10^{-5}, \mathfrak{p}_2 = 0.001542, \mathfrak{p}_1 = -0.0618, \mathfrak{p}_o = 0.957$ for $\theta \leq 40°$; $\mathfrak{p}_3 = -6.654 \times 10^{-7}, \mathfrak{p}_2 = 0.0001581, \mathfrak{p}_1 = -0.0127, \mathfrak{p}_o = 0.348$ for $40° < \theta \leq 85°$. The R-square value for this fitting is 0.9909. Using these approximations, (5) can be written as,

$$
\begin{aligned}
&(20 \cdot \mathfrak{q}_3 + a \cdot \mathfrak{p}_3) \cdot \theta^3 + (20 \cdot \mathfrak{q}_2 + a \cdot \mathfrak{p}_2) \cdot \theta^2 + \\
&(20 \cdot \mathfrak{q}_1 + a \cdot \mathfrak{p}_1) \cdot \theta + (20 \cdot \mathfrak{q}_o + a \cdot \mathfrak{p}_o) \\
&\leq P_{tx} - P_o - 20 \cdot \log_{10}(h_0) - 20 \cdot \log_{10}(f) + \\
&10 \cdot \log_{10}(G_{tx} \cdot G_{rx}) - 32.44.
\end{aligned}
\tag{6}
$$

This is a cubic equation, and its roots can be easily found in closed-form equation. The cubic equation has either one real root with two complex conjugate roots or three real roots. We have investigated the discriminant of this cubic equation and is negative for all possible range of heights, which indicates that, it has one real root with two complex roots. For brevity, closed form expression of the root of cubic equation (6) is omitted. Note that, the expression of real root of a generalized cubic equation $\theta^3 + \mathfrak{a} \cdot \theta^2 + \mathfrak{b} \cdot \theta + \mathfrak{c} = 0$ is given as [36]: $\theta_{real} = \left(-\frac{\mathfrak{B}}{2} + \sqrt{\frac{\mathfrak{B}^2}{4} + \frac{\mathfrak{A}^3}{27}} \right)^{\frac{1}{3}} + \left(-\frac{\mathfrak{B}}{2} - \sqrt{\frac{\mathfrak{B}^2}{4} + \frac{\mathfrak{A}^3}{27}} \right)^{\frac{1}{3}}$; where $\mathfrak{A} = \frac{3 \cdot \mathfrak{b} - \mathfrak{a}^2}{3}$ and $\mathfrak{B} = \frac{2 \cdot \mathfrak{a}^3 - 9 \cdot \mathfrak{a} \cdot \mathfrak{b} + 27 \cdot \mathfrak{c}}{27}$. If θ^* be the real root, which is the solution of the cubic equation in (6); then, the radius of RFET zone is given as: $R_{\text{RFET zone}} = h_0 / \tan(\theta^*)$.

Conversely, consider the case when area of RFET zone is fixed with a radius r_o and UAV hovers over a fixed ground location that is the center of the RFET zone. In this case, there is a range of possible UAV deployment height, such that the sensor nodes within RFET zone are able to harvest energy. There is also an optimal height of UAV in this height range. They are obtained from: $\mathbb{E}[L(h, \theta)] \leq P_{tx} - P_o$ with $\tan\theta = h/r_o$. The optimal deployment height of UAV can be obtained numerically by minimizing $\mathbb{E}[L(h, \theta)] - P_{tx} + P_o$ using Golden section method [35] due to the unimodal property proved in Lemma 2. Analytically, it can be obtained from: $\frac{\partial}{\partial h}\mathbb{E}[L(h, \theta)] = 0 \Rightarrow \pi \tan(\theta) + a \cdot b \cdot 9 \cdot \ln 10 \cdot \exp(b \cdot \theta)$. $\exp(b \cdot \theta)$ is approximated above and $\tan\theta$ cab be approximated as: $\tan(\theta) \approx \mathfrak{r}_3 \cdot \theta^3 + \mathfrak{r}_2 \cdot \theta^2 + \mathfrak{r}_1 \cdot \theta + \mathfrak{r}_o$ with $\mathfrak{r}_3 = 3.388 \times 10^{-6}, \mathfrak{r}_2 = -6.972 \times 10^{-5}, \mathfrak{r}_1 = 0.01842, \mathfrak{r}_o = -0.003959$ for $\theta \leq 40°$; with $\mathfrak{r}_3 = 0.0003219, \mathfrak{r}_2 = -0.05352, \mathfrak{r}_1 = 2.967, \mathfrak{r}_o = -53.31$ for $40° < \theta \leq 85°$. The R-square value for this fitting is 0.9894. This leads to a cubic equation, and its root can be obtained in closed form. Let θ_{opt} be the optimal elevation angle with respect to the periphery of the RFET zone, then $h_{opt} = r_o \tan(\theta_{opt})$. Using this optimal height, the possible range of deployment height can also be obtained

by solving $\mathbb{E}[L(h, \theta)] - P_{tx} + P_o = 0$, which has two roots around the optimal height due to unimodal nature. The roots can be obtained numerically using bisection method over two intervals around optimal height, and each interval will have a root. The height range between these roots correspond to the possible deployment height of UAV. Analytically, this can be obtained by using the approximation of $\log_{10}(\sec(\theta))$ as: $\log_{10}(\sec(\theta)) \approx \mathfrak{s}_3 \cdot \theta^3 + \mathfrak{s}_2 \cdot \theta^2 + \mathfrak{s}_1 \cdot \theta + \mathfrak{s}_o$ with $\mathfrak{s}_3 = 3.951 \times 10^{-6}, \mathfrak{s}_2 = 0.0005254, \mathfrak{s}_1 = 0.001739, \mathfrak{s}_4 = -0.006814$ for $\theta \leq 40°$; $\mathfrak{s}_3 = 0.0001338, \mathfrak{s}_2 = -0.02049, \mathfrak{s}_1 = 1.13, \mathfrak{s}_4 = -19.99$ for $40° < \theta \leq 85°$. The R-square value of fitting is 0.9926. This leads to the cubic equation, and the roots can be obtained in closed form.

C. Effective Power Harvested at Field Sensor Nodes

Even though the RFET zone is defined, the exact value of power available to each sensor node situated at different locations is unknown. Two main factors influencing the amount of harvested energy are the shadow statistics of the path loss and received power dependent variable RF-to-DC rectification efficiency of the energy harvester.

Actual harvested power depends on RF-to-DC rectification efficiency, which is a function of received RF power. Using the rectification efficiency values given in data sheet of power harvester [24], the harvested power $P_{\mathcal{H}}(\rho)$ is found to vary with input received power ρ as follows:

$$
P_{\mathcal{H}}(\rho) = \begin{cases} 0, & \text{if } \rho < \rho_o \\ \sum\limits_{i=0}^{2} w_i \cdot (\rho)^i, & \text{otherwise} \end{cases}
\tag{7}
$$

where $\rho_o = 10^{\frac{P_o}{10}}$ W, and w_i's are fitting coefficients: $w_0 = -4.858 \times 10^{-5}$, $w_1 = 0.5875$, $w_2 = -7.564$. The R-square value of the fitted function is 0.9996, which indicates excellent fitting.

Harvested power in expected sense captures the randomness caused by excess path loss due to long time of operation in RFET. The expected harvested power $P_{sen}(h, \theta)$ at a sensor node making an elevation angle θ with UAV hovering at altitude h is expressed as,

$$
\begin{aligned}
P_{sen}(h, \theta) &= \int_{\rho \geq \rho_o} P_{\mathcal{H}}(\rho) \cdot f_{P_{rx}(h, \theta)}(\rho) \cdot d\rho \\
&= \int_{\rho \geq \rho_o} (w_0 + w_1 \cdot \rho + w_2 \cdot \rho^2) \cdot f_{P_{rx}(h, \theta)}(\rho) \cdot d\rho \\
&= \eta_0 + \eta_1 + \eta_2
\end{aligned}
\tag{8}
$$

where ρ_o is the sensitivity of power harvester. $f_{P_{rx}(h, \theta)}(\rho)$ denotes the distribution of received power on linear scale (in Watts) at location (h, θ), which is expressed as:

$$
\begin{aligned}
f_{P_{rx}(h, \theta)}(\rho) = &\frac{10}{\rho\sqrt{2\pi}\sigma(\theta)\ln(10)} \cdot \\
&\exp\left[-\frac{(10\log_{10}(\rho) - P_{tx} + L_{fs}(h, \theta) + \mu(\theta))^2}{2\sigma^2(\theta)} \right]
\end{aligned}
\tag{9}
$$

The cumulative distribution function (CDF) of received power is obtained as: $F_{P_{rx}(h, \theta)}(\rho) =$
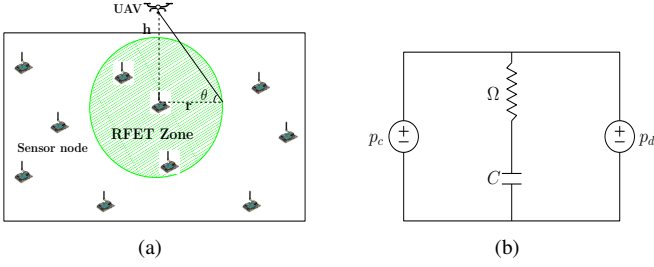
Figure 2: (a) System model for UAV-assisted charging; and (b) depiction of circuit operation at sensor node.
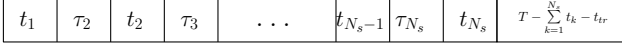
Figure 3: Realization of time vector.

$1 - Q\left(\frac{10\log_{10}\rho_o - P_{tx} + L_{fs}(h,\theta) + \mu(\theta)}{\sigma(\theta)}\right)$, where $Q(\cdot)$ is the Gaussian Q-function.

η_0, η_1, and η_2 are obtained as:

$$\eta_0 = w_0 \cdot Q(\kappa_0), \text{ with } \kappa_0 = \frac{10\log_{10}\rho_o - P_{tx} + L_{fs}(h,\theta) + \mu(\theta)}{\sigma(\theta)},$$

$$\eta_1 = w_1 \cdot \exp\left[\begin{array}{c}(P_{tx} - L_{fs}(h,\theta) - \mu(\theta)) \cdot \frac{\ln 10}{10} + \\ \frac{\sigma^2(\theta)}{2}\left(\frac{\ln 10}{10}\right)^2\end{array}\right] \cdot Q(\kappa_1),$$

$$\text{with } \kappa_1 = \frac{10\log_{10}\rho_o - P_{tx} + L_{fs}(h,\theta) + \mu(\theta) - \frac{\sigma^2(\theta)\ln 10}{10}}{\sigma(\theta)},$$

$$\eta_2 = w_2 \cdot \exp\left[\begin{array}{c}2(P_{tx} - L_{fs}(h,\theta) - \mu(\theta))\frac{\ln 10}{10} + \\ \frac{\sigma^2(\theta)}{2}\left(\frac{2\ln 10}{10}\right)^2\end{array}\right] \cdot Q(\kappa_2),$$

$$\text{with } \kappa_2 = \frac{10\log_{10}\rho_o - P_{tx} + L_{fs}(h,\theta) + \mu(\theta) - 2\frac{\sigma^2(\theta)\ln 10}{10}}{\sigma(\theta)}.$$

III. UAV MOBILITY OPTIMIZATION FOR CHARGING MULTIPLE FIELD SENSOR NODES

In the previous section on formulation of RFET zone, the power harvested at sensor nodes situated at different locations are obtained when UAV hovers at an altitude, which plays a key role while designing the charging mechanism. Consider a scenario as shown in Fig. 2 (a), where N_S sensor nodes are deployed in a given area A, and the sensor nodes are to be charged by UAV hovering at a given altitude. The harvested energy is stored in the supercapacitor. Fig. 2(b) shows the charging-discharging process of supercapacitor. The supercapacitor operates in a predefined voltage range, and sensor node dissipates energy with time in different operations like sensing, processing, and communication. If the power harvested is greater than energy dissipation rate, then the supercapacitor has surplus energy stored in it. On the other hand, if the power harvested is lesser than energy dissipation rate, then the supercapacitor's energy is dissipated. Charging rate, which is the effective power available to the sensor nodes, is decided by the relative location of sensor nodes and deployment height of UAV as discussed in the Section II (cf.

(8)). When UAV charges a particular node from height h just above it, the other nodes in the RFET zone also receive power depending on the path loss to these nodes.

UAV hovers just above the sensor node to perform RFET, because the harvested power is maximum at this hovering position in presence of shadow fading and non-linear rectification efficiency. The distance between transceiver as well as the effect of shadow fading is minimum in this orientation. This observation is in contrast with that in [37], where hovering of UAV above a group of ground-deployed sensor nodes was noted to be efficient for information transfer. This is because, in RFET, while hovering at different position other than just above the sensor node, the path loss as well as shadow fading increases significantly due to increase of separation between the RF transmitter and receiver. Thus, sensor nodes receive less power, and hence harvest less power. The change in distance between the RF transmitter and receiver affects the energy transfer efficiency more severely than information transfer due to difference in their sensitivities.

Let UAV hovers above k^{th} sensor node having initial voltage v_I^k and energy dissipation rate p_{d_k}, for a duration t_k. The initial voltage as well as the location of each sensor node is known to UAV from a centralized location before starting the charging process. With this system model, our aim is to minimize the total time of charging for a given set of field sensor nodes, which includes the time of charging the sensor nodes and travel time to visit them. The optimization problem is formulated as follows:

$$(\mathbf{P}): \underset{t_i,\, x_{ij}}{\text{minimize}} \quad \sum_{i=1}^{N_S} t_i + \frac{1}{\mathcal{U}}\sum_{i=1}^{N_S}\sum_{j=1}^{N_S} x_{ij}d_{ij}$$

subject to:

$$(C1) \quad v_F^k(v_I^k, \underline{p}^k, \underline{t}) \geq v_{th}^k, \ \forall k, k = 1, \cdots, N_S$$

$$(C2) \quad v_F^k(v_I^k, \underline{p}^k, \underline{t}) \leq v_{max}^k, \ \forall k, k = 1, \cdots, N_S$$

$$(C3) \quad \sum_{k=1}^{N_S} t_k \leq T - t_{tr}$$

$$(C4) \quad t_k \geq 0, \quad \forall k, \ k = 1, \cdots, N_S$$

$$(C5) \quad \sum_{j=1}^{N_S} x_{ij} = 1, \quad i \neq j$$

$$(C6) \quad \sum_{i=1}^{N_S} x_{ij} = 1, \quad i \neq j$$

$$(C7) \quad \sum_{i,j \in \mathcal{R}} x_{ij} \leq |\mathcal{R}| - 1, \ \mathcal{R} \subset \{2, \cdots, N_S\},$$
$$|\mathcal{R}| \geq 2$$

$$(C8) \quad x_{ij} = 0 \text{ or } 1. \tag{10}$$

The supercapacitor operates in predefined range of voltage level, which are captured in constraint (C1) and (C2). $\underline{p}^k$ is the power exchange vector of kth sensor node over time vector $\underline{t}$. The length of both vectors $\underline{p}^k$ and $\underline{t}$ are $2 \cdot N_S$, and the variation of $\underline{t}$ is shown in Fig. 3. The time vector for each sensor node is the same, whereas power vector $\underline{p}^k$ for each sensor node is different, which depends upon energy dissipation profile of sensor node, spatial arrangement of sensor nodes, and

charging sequence. If the UAV hovers above a sensor node, the other sensor nodes within the RFET zone also harvest power based on relative separation between the UAV transmitter and the sensor nodes. Hence charging and discharging occur simultaneously in these sensor nodes. This may be visualized from Fig. 2(b), where the operation of power harvester circuit is shown. The sensor nodes lying outside the RFET zone do not receive energy. Hence, discharging of battery energy occurs at those nodes in that epoch. $v_F^k(\cdot)$ is the final voltage level of kth sensor node having initial voltage v_I^k and goes through power exchange vector $\underline{p}^k$ over time vector $\underline{t}$. It is important to evaluate the power exchange vector $\underline{p}^k$.

Let $\mathfrak{N}_k$ denotes the set of sensor nodes, which are within the RFET zone around the kth sensor. k^{th} sensor itself is a default member of $\mathfrak{N}_k$. Therefore, the jth element of power exchange vector of kth sensor node, p_j^k is given as:

$$p_j^k = \begin{cases} -p_{d_k}, & \text{if } j \notin \mathfrak{N}_k \ \& \ j \bmod 2 \neq 0 \\ \gamma_{jk} - p_{d_k}, & \text{if } j \in \mathfrak{N}_k \ \& \ j \bmod 2 \neq 0 \\ -p_{d_k}, & \text{if } j \bmod 2 = 0 \end{cases} \quad (11)$$

where γ_{jk} is the power received at sensor node k when UAV hovers above sensor node j, and can be obtained from (8).

Constraint (C3) indicates the total time spent in charging process, which includes charging time and travel time; it should not exceed the target operational time of each sensor node, i.e., T. It is composed of charging time t_k, traveling time τ_k, and vacation time (last element of $\underline{t}$ indicates the vacation time, $t_{2 \cdot N_S} = T - t_{tr} - \sum_{i=1}^{N_S} t_i$). Vacation time refers to the time duration over which the charging process by UAV is not carried out. τ_k is the time elapsed in traveling from sensor node $k-1$ to k with $\tau_1 = 0$ (i.e., for the starting node). τ_k depends on the visiting sequence of sensor nodes with $\tau_k = \frac{d_{k-1,k}}{\mathcal{U}}$, where $d_{k-1,k}$ is the distance between $(k-1)^{\text{st}}$ to k^{th} sensor node, and $\mathcal{U}$ is the speed of UAV. $t_{tr} = \sum_{k=1}^{N_S} \tau_k$ is the total travel time. It is considered that UAV-mounted transmitter does not radiate power while traveling. This assumption does not alter the performance significantly, because the travel time is very small compared to the charging time[1]. Constraint (C4) corresponds to the non-negative nature of individual sensor's charging time.

Constraint (C5) and (C6) ensure that every node has one successor and one predecessor. (C8) $x_{ij} \in \{0, 1\}$ is binary variable taking the value 1 when node j is charged after node i, and 0 otherwise. Constraint (C7) ensures the elimination of cycles during the charging process. d_{ij} is the distance between sensor nodes i and j.

The problem at hand is to obtain the optimal solution of problem (**P**), which comprises of travel time and charging time. It is notable that, the constraints related to binary variable (i.e., (C5) - (C8)) do not overlap with the constraints of the continuous variables (i.e., (C1) - (C4)), whereas the constraints of continuous variable (i.e., (C3)) depend on the binary variable (i.e., $t_{tr} = \frac{1}{\mathcal{U}} \sum_{i=1}^{N_S} \sum_{j=1}^{N_S} x_{ij} d_{ij}$). With this observation, the optimization problem (**P**) can be decomposed

---

---

into two sub-problems and can be solved individually in the sequential way [38]. The overall optimal solution consists of optimal solution of each sub-problem. The solution of first sub-problem is plugged in the constraint (i.e., (C3)) of second sub-problem and then solved. The first sub-problem is stated as,

$$\textbf{(P1):} \quad \underset{x_{ij}}{\text{minimize}} \quad \frac{1}{\mathcal{U}} \sum_{i=1}^{N_S} \sum_{j=1}^{N_S} x_{ij} d_{ij}, \quad (11)$$

$$\text{subject to:} \quad (C5), \ (C6), \ \text{and} \ (C8).$$

This sub-problem evaluates the sequence of visiting the sensor nodes with minimum time spent in traveling. Using this sequence, the power exchange vector $\underline{p}^k$ is obtained from (11).

The second sub-problem is stated as,

$$\textbf{(P2):} \quad \underset{t_i}{\text{minimize}} \sum_{i=1}^{N_S} t_i, \quad (12)$$

$$\text{subject to:} \quad (C1), \ (C2), \ (C3), \ \text{and} \ (C4).$$

This sub-problem evaluates the optimal charging time required for each sensor node.

A. Optimal Solution of Problem P1

UAV charges the sensor nodes one by one, so it is important to obtain the order in which the nodes are going to be charged. UAV wants to minimize the total distance traveled or total travel time of the process, while deciding the order of charging. This optimization problem to find the shortest route is known as Traveling Salesman Problem (TSP) [39]. So, the optimization problem (**P1**) is TSP. TSP is known to be an NP-hard problem, but several polynomial time approximation methods are reported in the literature. Here, Hungarian method is used to solve the TSP, whose computational complexity is $O(n^3)$.

In standard TSP, the initial node (entry node) and final node (exit node) are same. But, if the initial and final nodes are not same then, this problem can be easily transformed to standard TSP by introducing a dummy node, say $(N_S + 1)^{\text{th}}$ node [39]. The distance of all existing nodes to this dummy node is 0, i.e., $d_{N_S+1,i} = d_{i,N_S+1} = 0, \ \forall i \in 1, \cdots, N_S$. Then the traveling sequence is evaluated for these $N_S + 1$ sensor nodes setting and finally the two virtual edges associated with dummy node are removed.

B. Optimal Solution of Problem P2

To solve (**P2**), it is important to evaluate the final voltage level $v_F(\cdot, \cdot, \cdot)$. The final voltage of supercapacitor embedded in sensor node after constant power charging/discharging depends upon the charging/discharging rate, time of charging, and initial voltage level of supercapacitor [40], [41]. Let the capacitance of supercapacitor is C farad and equivalent series resistance is Ω ohm for the harvester circuit shown in Fig. 2(b). Here, a supercapacitor of capacitance $C = 40$ farad and equivalent series resistance $\Omega = 0.15$ ohm are considered for analysis and performance results.

1) Equivalent Charging Process: The final voltage level of supercapacitor after time $\mathcal{T}$, when charged with constant power p_c having initial voltage v_I, is given as,

$$v_F(v_I, p_c, \mathcal{T}) = z_f^c \sqrt{\frac{4 \cdot p_c \cdot \Omega \cdot C^2}{2 \cdot z_f^c + 1}} \qquad (13)$$

where $z_f^c = \frac{1}{2}\left[W_o\left(e^{\left(1 + 2\frac{(\mathcal{T} + G_c(v_I))}{\Omega \cdot C}\right)} \right) - 1 \right]$ with Lambert function $W_o(\cdot)$, $G_c(v_I) = \Omega \cdot C \cdot [z_i^c + \frac{1}{2}\ln(1 + 2 \cdot z_i^c)]$, and $z_i^c = \frac{v_I^2 + v_I \sqrt{v_I^2 + 4 \cdot p_c \cdot \Omega}}{4 \cdot p_c \cdot \Omega}$.

The expressions of final voltage level involves the Lambert function, which makes the optimization problem (**P1**) analytically intractable. In this regard, an approximation of final voltage level is presented in the operational region of supercapacitor.

The operational voltage level of supercapacitor is [2.2 V, 3.8 V] [42], whereas the power harvested, p_c, in the given context lies in the range $[10 \times 10^{-6}\ \text{W}, 10 \times 10^{-3}\ \text{W}]$. With initial voltage $v_I \in [2.2\ \text{V}, 2.5\ \text{V}]$ and charging rate $p_c \in [10 \times 10^{-6}\ \text{W}, 10 \times 10^{-3}\ \text{W}]$, the variation of final voltage level is modeled using linear regression. Final voltage level is found to fit as a function of initial voltage level, charging rate, and time as follows:

$$v_F(v_I, p_c, t) = v_I + g_c(p_c) \cdot t, \quad g_c(p_c) = g_{co} + g_{c1} \cdot p_c \quad (14)$$

where $g_{co} = 2.711 \times 10^{-6}$, and $g_{c1} = 8.863 \times 10^{-3}$. The R-square value is 0.9930, which lies within the acceptable range of fitting [43]. The variation of voltage level against time for different initial voltage and charging rate are shown in Fig. 4(a), which also demonstrate the accuracy of approximation.

2) Equivalent Discharging Process: The final voltage level of supercapacitor after time $\mathcal{T}$, when discharged with constant power p_d having initial voltage v_I is given as,

$$v_F(v_I, -p_d, \mathcal{T}) = -z_f^d \sqrt{\frac{4 \cdot p_d \cdot \Omega \cdot C^2}{2 \cdot z_f^d + 1}} \qquad (15)$$

where $z_f^d = \frac{1}{2}\left[W_o\left(e^{\left(1 + 2\frac{(\mathcal{T} + G_d(v_I))}{\Omega \cdot C}\right)} \right) - 1 \right]$ with Lambert function $W_o(\cdot)$, $G_d(v_I) = \Omega \cdot C \cdot [z_i^d + \frac{1}{2}\ln(1 + 2 \cdot z_i^d)]$, and $z_i^d = \frac{v_I^2 + v_I \sqrt{v_I^2 - 4 \cdot p_d \cdot \Omega}}{4 \cdot p_d \cdot \Omega}$.

The drain power p_d in the given context lies in the range $[0, p_d]$. Here $p_d \leq 8 \times 10^{-5}\ \text{W}$ is considered for analysis (cf. Section V). Thus, with initial voltage $v_I \in [2.3\ \text{V}, 3\ \text{V}]$ and discharging rate $p_d \in [0, 8 \times 10^{-5}\ \text{W}]$, the variation of final voltage level is modeled using linear regression. The discharging equation is found to fit as a function of initial voltage level, discharging rate, and time as follows:

$$v_F(v_I, -p_d, t) = v_I + g_d(p_d) \cdot t, \quad g_d(p_d) = g_{do} + g_{d1} \cdot p_d \quad (16)$$

Here $g_{do} = 1.522 \times 10^{-9}$, and $g_{d1} = -0.01054$. The R-square value is 0.9916, which is in the acceptable range [43]. The variation of voltage level with time for different initial voltage and discharging rate in Fig. 4(b) proves the accuracy of approximation.
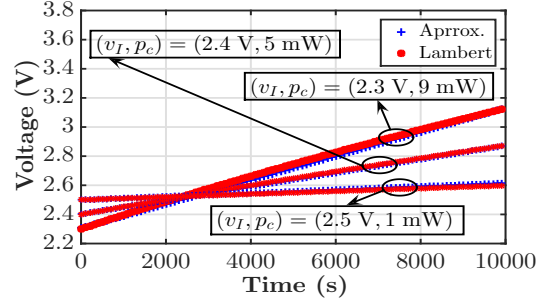
(a) Charging
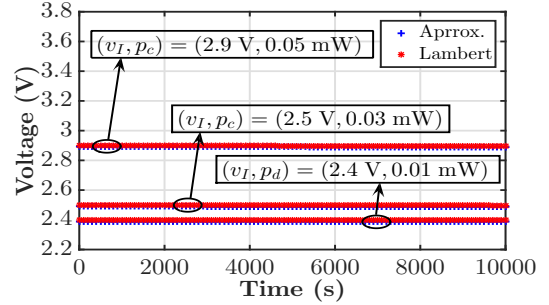
(b) Discharging

Figure 4: Variation of original and fitted values of voltage with time for (a) charging, and (b) discharging process.

Remark 2. *If the capacitor is consequently charged for time t_1 and t_2 with charging rate p_{c_1} and p_{c_2}, respectively, with initial voltage v_I, the final voltage is given by:*

$$v_F(v_I, [p_{c_1}, p_{c_2}], [t_1, t_2]) = v_I + g_c(p_{c_1}) \cdot t_1 + g_c(p_{c_2}) \cdot t_2. \quad (17)$$

Remark 3. *If the capacitor is consequently discharged for time t_1 and t_2 with discharging rate p_{d_1} and p_{d_2}, respectively, with initial voltage v_I, then the final voltage is:*

$$v_F(v_I, [-p_{d_1}, -p_{d_2}], [t_1, t_2]) = v_I + g_d(p_{d_1}) \cdot t_1 + g_d(p_{d_2}) \cdot t_2. \quad (18)$$

Remark 4. *If the capacitor is consequently charged for time t_1 with charging rate p_c and discharged for time t_2 with discharging rate p_d with initial voltage v_I. Then the final voltage is:*

$$v_F(v_I, [p_c, -p_d], [t_1, t_2]) = v_I + g_c(p_c) \cdot t_1 + g_d(p_d) \cdot t_2. \quad (19)$$

The remarks 2, 3, and 4 transform the constraints (C1) and (C2) into a linear function. This makes the problem (**P2**) a linear program. Hence, the optimal charging time for which UAV hovers above each sensor node can be obtained by solving it using linear programming [35].

IV. PROPOSED VOLTAGE AND OPERATIONAL TIME AWARE CHARGING MECHANISM

A supercapacitor operates in a predefined voltage range, and some amount of energy is kept safe for emergency situation. The normal operational range is above this safe margin, and upto the maximum allowed voltage level. The three operational region of a sensor node can be categorized as: healthy, unhealthy, and dead. $[v_{th}^k, v_{max}^k]$ is the healthy

range of operation, where sensor node normally functions. In unhealthy region $[v_{min}^k, v_{th}^k]$, the sensor node enters in critical mode of operation and usually this portion of energy is stored for emergency usage. If the voltage level of sensor node falls below v_{min}^k, then it becomes dead, which is undesirable. The sensor nodes are desired to operate in normal healthy region and hence, the number of healthy nodes among all the deployed sensor nodes is of our interest.

When UAV arrives for charging, the sensor nodes have different initial voltage levels and in these circumstances, the charging sequence plays a significant role. Minimizing the distance traveled is the only criteria in TSP. TSP does not consider the sensor node's health parameter, such as initial voltage level or power consumption profile, which have strong impact on the performance. *The sequence in which sensor nodes should be charged by UAV, such that, the unhealthy state of sensor nodes can be avoided*, is a very important issue. Keeping this in mind, different charging schemes are presented in this section, where the sensor node's health parameters are taken into consideration.

A. Voltage-aware Charging Sequence (VCS)

The sensor nodes are sorted according to their ascending order of voltage level, i.e., from minimum to maximum in *Voltage-aware Charging Sequence (VCS)*. The power exchange vector is obtained from (11) using this charging sequence. Then, the charging time required to charge each sensor node is obtained by solving (P2).

Sensor nodes are charged sequentially; the nodes have to wait for their turn. For a node with z^{th} position in the visiting sequence, the waiting time consists of travel time and charging time of the predecessor nodes. The waiting time vector $\underline{t}_w^z$ can be envisioned from Fig. 3. The power exchange vector of sensor node at z^{th} position during waiting time $\underline{p}_w^z$ is obtained from (11). The role of $\underline{p}_w^z$ is important because the sensor nodes lying in RFET zone will also receive power for their recharging. If the voltage level of sensor node during waiting time does not fall below a threshold voltage, i.e., $v_F(v_I^z, \underline{p}_w^z, \underline{t}_w^z) \geq v_{th}^z$, it is said to be healthy.

B. Operational Time-aware Charging Sequence (TCS)

VCS works well in homogeneous sensor deployment, where all sensor nodes have the same power consumption profile. It is not efficient in heterogeneous deployment scenario due to diverse power consumption profile. To this end, a charging scheme based on operational time, namely, *Operational Time-aware Charging Sequence (TCS)* is proposed. The operational time of zth sensor node ($_Ot^z$) with initial voltage level v_I^z, and power consumption p_d^z is obtained by solving: $v_F^z(v_I^z, -p_d^z, _Ot^z) = v_{th}^z$. The charging sequence is prepared according to the operational time in ascending order. The power exchange vector is obtained from (11) using this sequence and the charging time allocated to each sensor node is obtained by solving (**P2**).

C. Iterative Charging Sequence (ICS)

In the previous schemes (*TSP, VCS, TCS*), the sensor nodes are visited once and charged one by one for allocated amount of time. The performance with these schemes become worse when the charging time is higher than the operational time. Therefore, it requires mechanism to address this situation and hence, an iterative charging mechanism, namely, *Iterative Charging Sequence (ICS)* is presented here to improve the performance. Significant improvement in the durability of sensor node after charging for some time and negligible travel time of UAV due to it's excellent mobility capability are motives behind this scheme. Here, the sensor nodes can be charged iteratively rather than charging once. The charging time can be accumulated in each round upto the time obtained by solving (**P2**). *How much charging time will be allocated to each sensor node in an iteration?* is the most important issue while designing the iterative charging scheme. To address this issue, an optimization problem $\mathcal{P}$ is formulated, which provides the time allocated in an iteration. Let $\mathcal{S}$ be the sequence of sensor nodes in ascending order of remaining operational time with $_Ot_{\mathcal{S}(1)}^n \leq \cdots \leq _Ot_{\mathcal{S}(|S|)}^n$ in n^{th} iteration. Let $_It_{\mathcal{S}(i)}^n$ be the time allocated in the nth iteration to sensor node $\mathcal{S}(i)$ having operational time $_Ot_{\mathcal{S}(i)}^n$. Then, the time allocated to each sensor node in n^{th} iteration is obtained by solving the following optimization problem,

$$(\mathcal{P}): \quad \text{maximize} \quad \sum_{i=1}^{|S|} {}_It_{\mathcal{S}(i)}^n$$

$$
\begin{aligned}
\text{subject to:} \quad & (\mathcal{C}1) \quad \sum_{i=1}^{k}({}_It_{\mathcal{S}(i)}^n + \tau_{\mathcal{S}(i)}) \leq {}_Ot_{\mathcal{S}(k+1)}^n, \\
& \qquad\quad \forall\, k = 1, \cdots, |S| - 1, \\
& (\mathcal{C}2) \quad v_F^{S(1)}(v_I^{S(1)}, \underline{p}^{\mathcal{S}(1)}, {}_I\underline{t}^n) \geq v_{th}^{S(1)}, \\
& (\mathcal{C}3) \quad {}_It_{\mathcal{S}(i)}^n \geq 0, \; \forall i, \; i = 1, \cdots, |S|. \\
& (\mathcal{C}4) \quad {}_It_{\mathcal{S}(i)}^n \leq t_{\mathcal{S}(i)}, \; \forall i, \; i = 1, \cdots, |S|.
\end{aligned}
\tag{20}
$$

Constraint ($\mathcal{C}1$) indicates that the time allocated to a particular sensor node in an iteration depends upon the remaining operational time of subsequent sensor nodes. This also includes the time elapsed in traveling (τ_i). Constraint ($\mathcal{C}2$) indicates that, the time should be allocated in an iteration such that the initial sensor node having minimum operational time should not enter into the unhealthy region. Constraint ($\mathcal{C}3$) corresponds to the non-negative time allocation. The last constraint ensures that time allotted in a single iteration is less than the total charging time for a particular node. Constraint ($\mathcal{C}4$) restricts the time allocated in each iteration.

The detailed procedure for *ICS* is mentioned in Algorithm 1. First of all, the sensor nodes are arranged according to *TCS*, and then using this sequence, charging time required by each node is calculated by solving (P2). A sensor node will be eliminated from iteration in two scenarios: either it goes into unhealthy region or it will be charged upto required time (obtained by solving (**P2**)). The charging time for each sensor node in individual iteration is obtained by solving ($\mathcal{P}$). The voltage level of sensor nodes are updated after charging each

sensor node due to effect of RFET zone. The time allocated in each iteration for sensor nodes are accumulated and updated, such that, the sensor nodes can be charged upto time obtained by solving (**P2**).

Algorithm 1 Iterative Charging Sequence (ICS)

1: Input: $\mathcal{S}$: Set of sensor nodes, N_S, Location of sensor nodes, Initial voltage level of sensor nodes, Power consumption profile of sensor nodes
2: Output: Number of healthy sensor nodes
3: Arrange the sensor nodes according to *TCS*
4: Find $t_{\mathcal{S}(i)}$; charging time required for sensor node from (**P2**)
5: Define $\mathcal{R} = \{\phi\}$: Set of unhealthy sensor nodes
6: Initialize: $n = 0$, $_It_{\mathcal{S}(i)}^{n=0} = 0 \ \forall i = 1, \cdots, |\mathcal{S}|$
7: **while** $\mathcal{S} \neq 0$ **do**
8:     Set $n = n + 1$; increment iteration number
9:     Find $_It_{\mathcal{S}(i)}^n$ by solving ($\mathcal{P}$)
10:     $_It_{\mathcal{S}(i)}^n = \min\{t_{\mathcal{S}}(i), \ _It_{\mathcal{S}(i)}^n\}$
11:     **for** $i = 1 : |\mathcal{S}|$ **do**
12:         Charge node $\mathcal{S}(i)$ and nodes lying in the RFET zone for time $_It_{\mathcal{S}(i)}^n$
13:         Update voltage level of the sensor nodes of sensor set $\mathcal{S}$
14:         $_It_{\mathcal{S}(i)}^n = _It_{\mathcal{S}(i)}^n + _It_{\mathcal{S}(i)}^{n-1}$
15:         **if** $_It_{\mathcal{S}(i)}^n == t_{\mathcal{S}(i)}$ **then**
16:           $\mathcal{S} = \mathcal{S} - \{\mathcal{S}(i)\}$
17:         **end if**
18:         **if** $v_F^{\mathcal{S}(i)} < v_{th}^{\mathcal{S}(i)}$ **then**
19:           $\mathcal{R} = \mathcal{R} \cup \{\mathcal{S}(i)\}$
20:           $\mathcal{S} = \mathcal{S} - \{\mathcal{S}(i)\}$
21:         **end if**
22:     **end for**
23:     Arrange sensor nodes of $\mathcal{S}$ according to *TCS*
24: **end while**
25: Number of healthy sensor nodes = $N_S - |\mathcal{R}|$

V. RESULTS AND DISCUSSIONS

In this section, UAV-assisted RFET performance is numerically evaluated. The sensor nodes are deployed in a given area according to Poisson point process. The initial voltage level of sensor nodes are uniformly distributed between 2.3 V and 2.4 V, whereas the threshold voltage is 2.3 V and the minimum allowed voltage level is 2.2 V. For performance analysis, the power transmission level of 4 W is considered. We have considered CO gas sensor having average energy dissipation rate 0.05 mW , i.e., $p_{d_i} = 0.05$ mW $\forall i$ in case of homogeneous sensor node deployment, which is sufficient for event driven and periodic reporting sensor nodes [1]. The values of other parameters are: $f = 0.915$ GHz, $P_o = -12$ dBm, $G_{tx} = 2.10$, $G_{rx} = 1.25$, $T = 24$ hrs, $\mathcal{U} = 10$ m/s.

A. Dimensioning of RFET Zone

Variation of radius of RFET zone against UAV deployment height is shown in Fig. 5(a). The plots show that, the radius
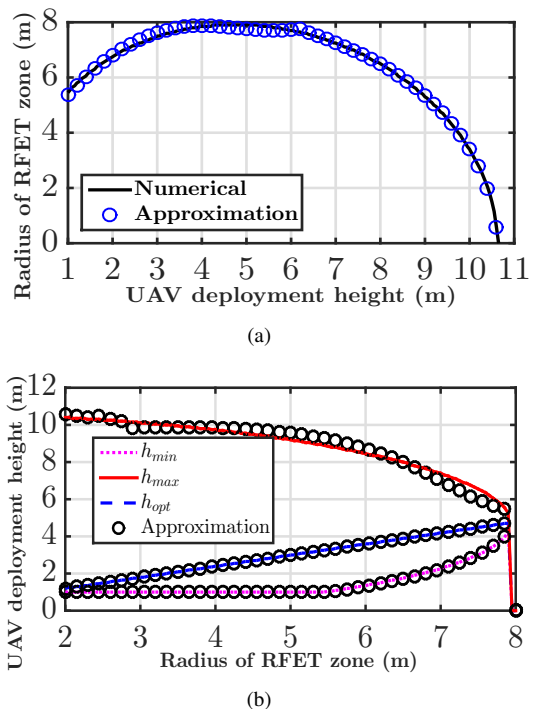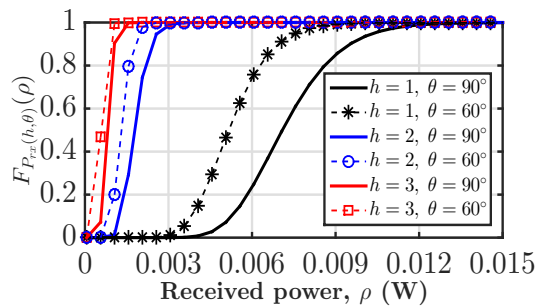

Figure 5: Variation of (a) radius of RFET zone against UAV deployment height, and (b) available height range against radius of RFET zone.

estimated using approximations closely matches with that obtained using numerical technique. The radius of RFET zone for a given deployment height indicates the non-decreasing nature of path loss, proved in Lemma 3; energy can be harvested up to this radius. It may be noted that, the radius of RFET zone increases up to some height, then it decreases, demonstrating its unimodal nature, as proved in Lemma 2. The radius becomes zero at a particular height, which is the maximum possible height for the UAV to facilitate RFET.

The variation of allowable height to facilitate UAV-assisted RFET along with the optimal height for a given RFET zone radius is shown in Fig. 5(b). The plots indicate that, the analytical approximations on deployment heights ($h_{min}, h_{opt}, h_{max}$) match well with the numerically computed exact values. The range of UAV deployment height is wider for lesser radius of RFET zone; this height range reduces and converges with increase in RFET zone radius due to increase in path loss.

The variation of CDF of received power level, $F_{P_{rx}(h,\theta)}(\rho)$, is shown in Fig. 6(a) for different deployment heights and different elevation angles. It can be observed that, more power is received at a higher elevation angle, which is because free space path loss as well as shadow parameters, i.e., mean and variance, are higher at smaller elevation angle.

Effective power harvested at a sensor node located at different positions (captured in (8)) is shown in Fig. 6(b) for different UAV deployment heights. As the elevation angle increases, the effective power available increases significantly, which validates the observation in Fig. 6(a). A sensor node harvests maximum power when UAV hovers just above it, i.e., when elevation angle is $90°$ (cf. Remark 1). The harvested power decreases with decrease in elevation angle due to increase in
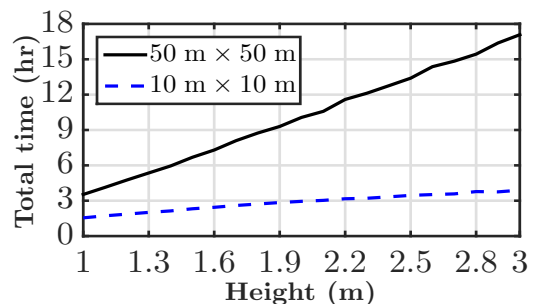
(a)
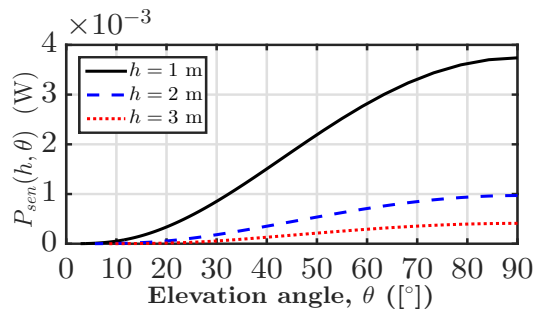
(b)

Figure 6: Variation of (a) CDF of received power level, and (b) effective power available against elevation angle for different UAV deployment heights.

(a)

(b)

Figure 7: Variation of total charging time against (a) UAV height with $N_S = 50$, and (b) number of sensor with $h = 1$ m.

path loss as well as shadow effects. The radius of RFET zone is: $R_{\text{RFET zone}} = h_o / \tan(\theta^*)$ with $\theta^* = 10.40°, 16.50°$, and $21.80°$ for $h_o = 1, 2$, and 3 m, respectively. It may be noted from Fig. 6(b) that, the energy harvested outside the RFET zone, i.e., when $\theta < \theta^*$, is negligible compared that to inside the RFET zone.

Remark 5. *The harvested power reduces significantly as the elevation angle decreases, and this is insignificant outside the RFET zone.*

B. Impact of RFET Zone

Two different deployment scenarios, one in an area 10 m × 10 m and the other in 50 m×50 m are considered to investigate the impact of RFET zone. The variation of total charging time against UAV deployment height is shown in Fig. 7(a). The charging time increases with increase in height, because the target sensor node over which UAV hovers as well as the neighborhood sensor nodes lying in RFET zone receive less power (cf. Fig. 6(b)). Also, the value of RF-to-direct current rectification efficiency is very small at lesser received power, which leads to the reduction in harvested power. Hence, the charging time increases with increase in UAV deployment height. This observation suggests that, the charging process by UAV should be carried out at altitude as low as possible. Further, the time elapsed to charge the sensor nodes is lesser in case of smaller area. This is because, with the same number of nodes deployed in a smaller area the RFET zone covers more number of nodes, which aids in simultaneous charging of the neighboring nodes.

The variation of charging time against number of deployed nodes is shown in Fig. 7 (b). It can be observed that, as the number of deployed sensor nodes increases, total charging time increases for both the deployment scenarios. However, with increased number of deployed sensor nodes, the rate of increase of charging time reduces significantly in smaller deployment area. This also happens due to the fact that, the RFET zone covers more sensor nodes in smaller deployment area. Therefore, more number of nodes in the RFET zone receive RF power, and are simultaneously recharged (cf. Fig. 6 (b)). This leads to reduction in total charging time of the field nodes in the deployment area.

Remark 6. *The number of sensor nodes lying in the RFET zone has strong impact on charging time due to simultaneous charging of nodes.*

C. Algorithm Performance with Different Charging Scheme

For this numerical study, UAV hovering altitude 1 m is considered. Simulation results on fraction of unhealthy nodes with different charging schemes (*TSP, VCS, TCS, ICS*), are presented.

Variation of fraction of unhealthy sensor nodes against the total number of deployed sensor nodes is shown in Fig. 8(a) with homogeneous power consumption profile of nodes. As the number of deployed nodes increases, fraction of unhealthy nodes increases in all schemes, but the performance is much severe in case of *TSP*. This indicates that, TSP is not the best option, which was the basic mobility planning in the previously reported works [15], [19], [22]. This is because, TSP does not take into consideration the remaining energy
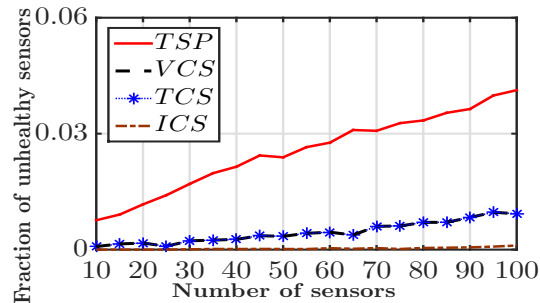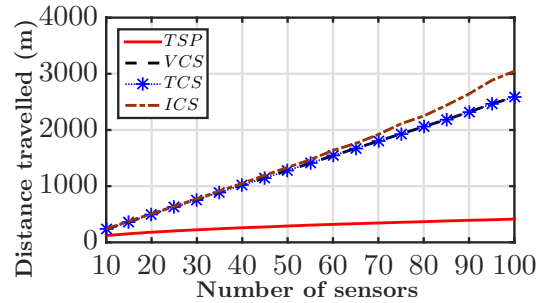
(a) Homogeneous
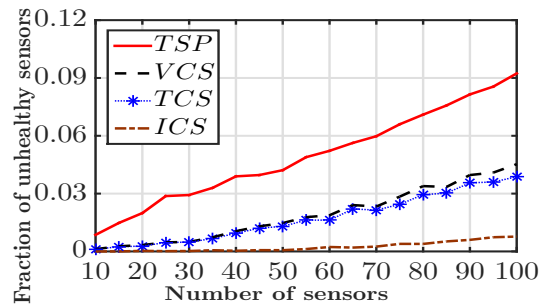
(b) Heterogeneous

Figure 8: Variation of fraction of unhealthy sensor nodes for (a) homogeneous, and (b) heterogeneous sensor deployment in 50 m × 50 m area.

(a) Homogeneous

(b) Heterogeneous

Figure 9: The distance traveled for different schemes in different deployment scenario in 50 m × 50 m area.

(a) Homogeneous

(b) Heterogeneous

Figure 10: Variation of fraction of unhealthy sensor nodes against deployment area with $N_S = 100$ for (a) homogeneous, and (b) heterogeneous sensor deployment.

levels of the deployed sensor nodes. Due to this, the sensor nodes having energy level close to the lower threshold deplete and become unhealthy. The performance of *VCS* and *TCS* nearly overlap due to homogeneous deployment, whereas *ICS* outperforms all the other three schemes.
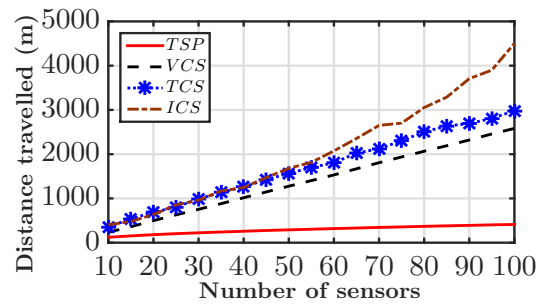
In heterogeneous node deployment scenario, four different type of sensor nodes (CO, H_2S, NO_2, and Cl_2) having respective power consumption profiles 0.05 mW, 0.06 mW, 0.07 mW, and 0.08 mW are considered. Fig. 8(b) shows the variation of fraction of unhealthy nodes for different schemes with heterogeneous sensor node deployment. Here also, the performance of *TSP* is worst compared to the other schemes. Unlike in homogeneous deployment scenario, here *TCS* outperforms *VCS*, because of diverse power consumption profile of the nodes. With heterogeneous sensor nodes, *ICS* performance is significantly better than the other schemes.

The total distance traveled is shown in Fig. 9 for different schemes in different deployment scenario. It may be observed that, the distance traveled is maximum in *ICS* scheme, which is marginally higher among the four proposed schemes: *TSP, VCS, TCS, ICS*, whereas the distance traveled is minimum in case of *TSP*. The distance traveled increases significantly with increase in number of deployed sensor nodes, as it has to travel more to charge more sensor nodes.

The variation of fraction of unhealthy sensor nodes for different deployment area (area = (side of square)^2) with 100 sensor nodes is shown in Figs. 10(a) and 10(b), respectively, for homogeneous and heterogeneous deployment scenarios. It may be noted that, the performance of all the four schemes are nearly identical for smaller deployment area. This is because the neighborhood se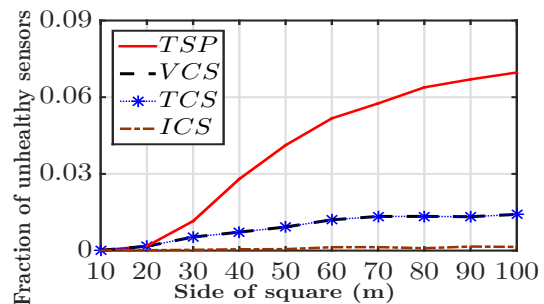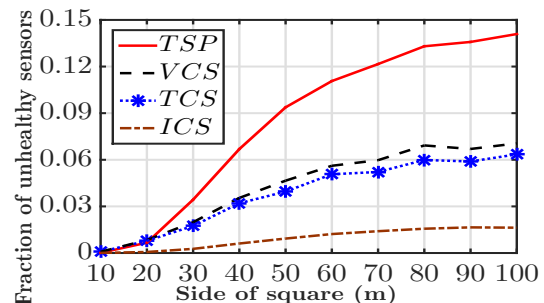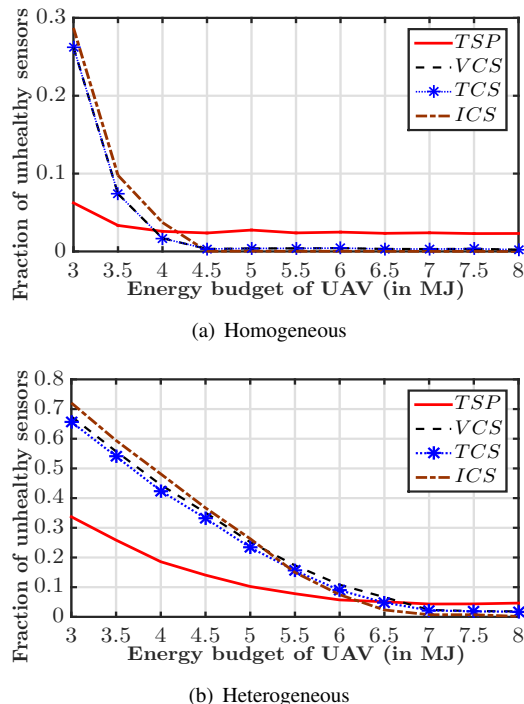nsor nodes lying in RFET zone harvest significant amount of energy due to simultaneous charging (cf. Remark 6), and they do not become unhealthy. Charging performance degrades with increase in deployment area, and *ICS* outperforms the other three schemes in both deployment scenarios. As the deployment area increases, simultaneous

(a) Homogeneous

(b) Heterogeneous

Figure 11: Variation of fraction of unhealthy sensor nodes against energy budget of UAV with $N_S = 50$ and area of deployment 50 m× 50 m for (a) homogeneous, and (b) heterogeneous sensor deployment.

charging is not effective, because less number of sensor nodes lie in RFET zone, and hence they become unhealthy.

Remark 7. *The performance of all the schemes are nearly identical when deployment area is smaller, whereas ICS outperforms all other schemes for larger deployment area.*

The energy limitation of UAV is not a severe issue; efforts toward longer operation of UAV [44]. Recently, several promising technologies like solar-powered quadcopters [45], fuel cell-powered UAV [46], efficient automatic battery replacement [47], and combustion engine-powered UAV [48], have been reported towards prolonging the UAV operational time. Time of flight up to several hours has been demonstrated in these works, which is well sufficient for our application.

However, the impact of energy budget of UAV on the performance is also investigated. The total energy budget of UAV in UAV-assisted RFET process accounts for energy consumed by UAV-mounted RF transmitter, and energy consumed during hovering or charging and traveling. Power consumed by UAV during charging is 214.44 W, whereas it consumes 214.44 W power during traveling with speed of 10 m/s from one node to other one [1]. The RF power transmission further consumes 5.33 W power [1]. With these data, the variation of fraction of unserved sensor nodes against the total energy budget of UAV when 50 sensor nodes deployed in 50 m×50 m area is shown in Fig. 11 for homogeneous and heterogeneous scenarios for different schemes with hovering altitude of 1 m. It may be noted from Fig. 11 that, the performance improves significantly with increase in energy budget of UAV for all the schemes, because the durability increases with increase of energy budget of UAV, and hence the performance enhances.

For a less energy budget, TSP performs better than the other schemes, because the energy-hungry nodes are charged in the beginning in TCS, VCS, and ICS schemes, which take relatively higher time and the nodes in the end are not served. Also, the energy consumption in traveling is minimum compared to the other schemes in TSP (see Fig. 9). Also, the energy-hungry nodes are charged in the beginning in TCS, VCS, and ICS schemes, which take relatively higher time and the nodes in the end are not served. Compared to TSP, the performance of TCS, VCS, and ICS improves drastically with increase of energy budget.

VI. CONCLUDING REMARKS

In this work, a new paradigm of wirelessly charging WSN nodes using UAV assisted RFET has been presented. A novel concept of RFET zone has been defined; all nodes located inside this zone are able to harvest energy. The analysis has accounted for the non-linear RF-to-DC conversion efficiency and shadowing statistics, which have strong impact on the effective power harvested at the sensor nodes situated at different locations. Based on this analysis, an optimization problem has been formulated to minimize the total time required to charge the on-board supercapacitor of the field sensor nodes. This problem has been decomposed into two sub-problems and solved in sequential steps. The first sub-problem provides the charging sequence, that offers minimum time to travel, which has been solved using TSP approach. In the second sub-problem, approximation for Lambert function has been presented to find the optimal charging time of each node. UAV-aided charging performance in terms of number of healthy sensor node, that can be supported for their uninterrupted operation, has been presented. To improve on the size of network, i.e., the number of field nodes that can be supported, three different schemes of charging sequence, namely, *Voltage-aware Charging Sequence (VCS)*, *Operational Time-aware Charging Sequence (TCS)*, and *Iterative Charging Sequence (ICS)* have been proposed and their respective performance has been analyzed. Through numerical results it has been demonstrated that, *TSP* based charging sequence is generally suboptimal.

Further investigations on study of multiple UAV coordination for RFET would be of future research interest. Additionally, the design of new charging protocols for enhanced performance is another interesting direction.

APPENDIX

A. Proof of Lemma 1

The Hessian matrix of expectation of path loss given in (3) is: $\mathcal{H}(h,r) = \begin{bmatrix} \frac{\delta^2 \mathbb{E}[L(r,h)]}{\delta r^2} & \frac{\delta^2 \mathbb{E}[L(r,h)]}{\delta r \delta h} \\ \frac{\delta^2 \mathbb{E}[L(r,h)]}{\delta h \delta r} & \frac{\delta^2 \mathbb{E}[L(r,h)]}{\delta h^2} \end{bmatrix}$. For a function to be convex, the Hessian matrix should positive semidefinite, i.e., $|\mathcal{H}(h,r)| \geq 0$.

The elements of Hessian matrix $\mathcal{H}(h,r)$ are given as:

$$\mathcal{H}(h,r)|_{11} = \frac{20}{((h^2+r^2))}\Big[\frac{1}{(\ln 10)} - \frac{2 \cdot r^2}{(\ln 10)\cdot(h^2+r^2)} +$$
$$\frac{18\cdot a \cdot b \cdot r \cdot h}{\pi \cdot (h^2+r^2)}\cdot\exp(b\cdot\frac{180}{\pi}\cdot\tan^{-1}(h/r)) +$$
$$\frac{1620\cdot a \cdot b^2\cdot h^2}{\pi^2\cdot r^2\cdot(\frac{h^2}{r^2}+1)}\cdot\exp(b\cdot\frac{180}{\pi}\cdot\tan^{-1}(h/r))\Big],$$

$$\mathcal{H}(h,r)|_{12} = \frac{20}{((h^2+r^2))}\Big[-\frac{2\cdot r \cdot h}{(\ln 10)\cdot(h^2+r^2)} -$$
$$\frac{18\cdot a \cdot b \cdot r^2}{\pi \cdot (h^2+r^2)}\cdot\exp(b\cdot\frac{180}{\pi}\tan^{-1}(h/r)) +$$
$$\frac{9\cdot a \cdot b}{\pi}\cdot\exp(b\cdot\frac{180}{\pi}\tan^{-1}(h/r)) +$$
$$\frac{1620\cdot a \cdot b^2\cdot h}{\pi^2\cdot r\cdot(\frac{h^2}{r^2}+1)}\cdot\exp(b\cdot\frac{180}{\pi}\cdot\tan^{-1}(h/r))\Big],$$

As the function $\mathbb{E}[L(r,h)]$ is continuous, $\mathcal{H}(h,r)|_{12} = \mathcal{H}(h,r)|_{21}$.

$$\mathcal{H}(h,r)|_{22} = \frac{20}{((h^2+r^2))}\Big[\frac{1}{(\ln 10)} - \frac{2\cdot h^2}{(\ln 10)\cdot(h^2+r^2)} +$$
$$\frac{18\cdot a \cdot b \cdot r \cdot h}{\pi \cdot (h^2+r^2)}\cdot\exp(b\cdot\frac{180}{\pi}\tan^{-1}(h/r)) +$$
$$+\frac{1620\cdot a \cdot b^2}{\pi^2 2\cdot(\frac{h^2}{r^2}+1)}\cdot\exp(b\cdot\frac{180}{\pi}\tan^{-1}(h/r))\Big].$$

The determinant $|\mathcal{H}(h,r)|$ is investigated numerically. It is noted that, the determinant is not always positive. Therefore, $\mathbb{E}[L(r,h)]$ is not a convex function of height and radius.

B. Proof of Lemma 2

For a function to be unimodal, the sign of derivative changes only once. The derivative of (3) with respect to height h for a constant r is found as:

$$\frac{\partial}{\partial h}\mathbb{E}[L(h,\theta)] = \frac{\partial}{\partial h}\Big[10\ \log_{10}(h^2+r^2) + a \cdot \exp(b\cdot\theta)\Big],$$
$$= \frac{20h}{(h^2+r^2)\ln 10} + \frac{180 a \cdot b}{\pi}\cdot\frac{r}{h^2+r^2}\cdot\exp(b\cdot\theta),$$
$$= \frac{r}{h^2+r^2}\cdot\frac{a \cdot b \cdot 180}{\pi}\Big[\frac{\pi}{a\cdot b\cdot 9\cdot\ln 10}\tan(\theta) +$$
$$\exp(b\cdot\theta)\Big] = \frac{r}{h^2+r^2}\cdot\frac{a\cdot b\cdot 180}{\pi}\cdot g(\theta),$$

where $g(\theta) = \frac{\pi\tan(\theta)}{a\cdot b\cdot 9\cdot\ln 10} + \exp(b\cdot\theta)$. To investigate the nature of $g(\theta)$, its derivative is given as:

$$g'(\theta) = \frac{180}{\pi}\cdot\frac{r}{h^2+r^2}\cdot b\cdot\exp(b\cdot\theta) + \frac{180}{\pi}\cdot\frac{r}{h^2+r^2}\cdot\frac{\pi\sec^2(\theta)}{a\cdot b\cdot 9\cdot\ln 10}.$$

$a > 0$ and $b < 0$ leads to $g'(\theta) < 0 \ \forall \theta \in [0,90]$, i.e., the function $g(\theta)$ is monotonically decreasing. $g(\theta)|_{\theta=0} > 0$, $g(\theta)|_{\theta=90} < 0$; this indicates that $g(\theta)$ will change sign only once, because it is a decreasing function. Therefore, $\frac{\partial}{\partial h}\mathbb{E}[L(h,\theta)]$ will also change sign only once, which proves its unimodal nature.

C. Proof of Lemma 3

For a function to be non-decreasing, the sign of derivative should be always non-negative. The derivative of expectation of path loss given in (3) with respect to radius, while treating height as constant, is: $\frac{\partial}{\partial r}\mathbb{E}[L(h,\theta)] = \frac{20}{\ln 10}\cdot\frac{r}{h^2+r^2} - a\cdot b\cdot\frac{180}{\pi}\cdot\exp(b\cdot\theta)\cdot\frac{h}{h^2+r^2}$. Observing the values of a and b ($a\cdot b < 0$), one can deduce that the quantity on right hand side of the above equation is always positive, which proves the non-decreasing nature of $\mathbb{E}[L(h,\theta)]$.

REFERENCES

[1] S. Suman, S. Kumar, and S. De, "UAV-assisted RF energy transfer," in *Proc. IEEE Int. Conf. Commun. (ICC)*, Kansas City, MO, USA, May, 2018, pp. 1–6.

[2] A. Al-Fuqaha, M. Guizani, M. Mohammadi, M. Aledhari, and M. Ayyash, "Internet of things: A survey on enabling technologies, protocols, and applications," *IEEE Commun. Surveys Tuts.*, vol. 17, no. 4, pp. 2347–2376, June 2015.

[3] A. P. Abidoye and I. C. Obagbuwa, "Models for integrating wireless sensor networks into the Internet of Things," *IET Wireless Sensor Syst.*, vol. 7, no. 3, pp. 65–72, May 2017.

[4] "Ericsson Mobility Report: On the pulse of the networked society," Nov. 2016.

[5] N. A. Pantazis, S. A. Nikolidakis, and D. D. Vergados, "Energy-efficient routing protocols in wireless sensor networks: A survey," *IEEE Commun. Surveys Tuts.*, vol. 15, no. 2, pp. 551–591, July 2013.

[6] P. Huang, L. Xiao, S. Soltani, M. W. Mutka, and N. Xi, "The evolution of MAC protocols in wireless sensor networks: A survey," *IEEE Commun. Surveys Tuts.*, vol. 15, no. 1, pp. 101–120, Apr. 2013.

[7] R. C. Shah, S. Roy, S. Jain, and W. Brunette, "Data MULEs: Modeling and analysis of a three-tier architecture for sparse sensor networks," *Elsevier Ad Hoc Net. J.*, vol. 1, no. 2, pp. 215 – 233, Sep. 2003.

[8] W. Wang, V. Srinivasan, and K. C. Chua, "Extending the lifetime of wireless sensor networks through mobile relays," *IEEE/ACM Trans. Netw.*, vol. 16, no. 5, pp. 1108–1120, Oct. 2008.

[9] S. R. Gandham, M. Dawande, R. Prakash, and S. Venkatesan, "Energy efficient schemes for wireless sensor networks with multiple mobile base stations," in *Proc. IEEE GLOBECOM*, San Francisco, CA, USA, Dec. 2003, pp. 377–381.

[10] P. Kamalinejad, C. Mahapatra, Z. Sheng, S. Mirabbasi, V. C. M. Leung, and Y. L. Guan, "Wireless energy harvesting for the Internet of Things," *IEEE Commun. Mag.*, vol. 53, no. 6, pp. 102–108, June 2015.

[11] S. De, A. Kawatra, and S. Chatterjee, "On the feasibility of network RF energy operated field sensors," in *IEEE ICC*, Cape Town, South Africa, May 2010, pp. 1–5.

[12] S. Suman and S. De, "Solar-enabled green base stations: Cost versus utility," in *Proc. IEEE WoWMoM*, Macau, China, June 2017, pp. 1–8.

[13] L. Xie, Y. Shi, Y. T. Hou, and A. Lou, "Wireless power transfer and applications to sensor networks," *IEEE Wireless Commun.*, vol. 20, no. 4, pp. 140–145, Aug. 2013.

[14] S. Saab, N. Kouzayha, J. Costantine, and Z. Dawy, "Positive impact of interference on RF energy harvesting for IoT devices," in *Proc. IEEE Int. Symp. PIMRC*, Bologna, Italy, Sep. 2018, pp. 312–317.

[15] L. Xie, Y. Shi, Y. T. Hou, and H. D. Sherali, "Making sensor networks immortal: An energy-renewal approach with wireless power transfer," *IEEE/ACM Trans. Netw.*, vol. 20, no. 6, pp. 1748–1761, Dec. 2012.

[16] C. Wang, J. Li, F. Ye, and Y. Yang, "A mobile data gathering framework for wireless rechargeable sensor networks with vehicle movement costs and capacity constraints," *IEEE Trans. Comput.*, vol. 65, no. 8, pp. 2411–2427, Aug. 2016.

[17] L. Xie, Y. Shi, Y. T. Hou, W. Lou, H. D. Sherali, and S. F. Midkiff, "On renewable sensor networks with wireless energy transfer: The multi-node case," in *Proc. IEEE SECON*, Seoul, South Korea, June 2012, pp. 10–18.

[18] B. Griffin and C. Detweiler, "Resonant wireless power transfer to ground sensors from a UAV," in *Proc. IEEE Int. Conf. Robot. Autom.*, Saint Paul, MN, USA, May 2012, pp. 2660–2665.

[19] S. De and R. Singhal, "Toward uninterrupted operation of wireless sensor networks," *IEEE Comp. Mag.*, vol. 45, no. 9, pp. 24–30, Sep. 2012.

[20] U. Baroudi, "Robot-assisted maintenance of wireless sensor networks using wireless energy transfer," *IEEE Sensors J.*, vol. 17, no. 14, pp. 4661–4671, July 2017.

[21] F. Sangare, Y. Xiao, D. Niyato, and Z. Han, "Mobile charging in wireless-powered sensor networks: Optimal scheduling and experimental implementation," *IEEE Trans. Veh. Technol.*, vol. 66, no. 8, pp. 7400–7410, Aug. 2017.

[22] L. Fu, L. He, P. Cheng, Y. Gu, J. Pan, and J. Chen, "ESync: Energy synchronized mobile charging in rechargeable wireless sensor networks," *IEEE Trans. Veh. Technol.*, vol. 65, no. 9, pp. 7415–7431, Sep. 2016.

[23] A. Kurs, A. Karalis, R. Moffatt, J. D. Joannopoulos, P. Fisher, and M. Soljačić, "Wireless power transfer via strongly coupled magnetic resonances," *Science*, vol. 317, no. 5834, pp. 83–86, July 2007.

[24] Powercast. [Online]. Available: http://www.powercastco.com

[25] H. Dai, Y. Liu, G. Chen, X. Wu, T. He, A. X. Liu, and H. Ma, "Safe charging for wireless power transfer," *IEEE/ACM Trans. Netw.*, vol. 25, no. 6, pp. 3531–3544, Dec. 2017.

[26] S. He, J. Chen, F. Jiang, D. K. Y. Yau, G. Xing, and Y. Sun, "Energy provisioning in wireless rechargeable sensor networks," *IEEE Trans. Mobile Comput.*, vol. 12, no. 10, pp. 1931–1942, Oct. 2013.

[27] J. Xu, Y. Zeng, and R. Zhang, "UAV-enabled wireless power transfer: Trajectory design and energy optimization," *IEEE Trans. Wireless Commun.*, vol. 17, no. 8, pp. 5092–5106, Aug. 2018.

[28] S. Hayat, E. Yanmaz, and R. Muzaffar, "Survey on unmanned aerial vehicle networks for civil applications: A communications viewpoint," *IEEE Commun. Surveys Tuts.*, vol. 18, no. 4, pp. 2624–2661, 4th Quart. 2016.

[29] S. Kumar, S. Suman, and S. De, "Backhaul and delay-aware placement of UAV-enabled base station," in *Proc. IEEE INFOCOM Wksp.*, Honolulu, HI, USA, Apr. 2018, pp. 634–639.

[30] D. Vasisht, Z. Kapetanovic, J. Won, X. Jin, R. Chandra, S. Sinha, A. Kapoor, M. Sudarshan, and S. Stratman, "Farmbeats: An IoT platform for data-driven agriculture," in *Proc. USENIX (NSDI)*, Boston, MA, USA, Mar. 2017, pp. 515–529.

[31] D. Floreano and R. J. Wood, "Science, technology and the future of small autonomous drones," *Nature*, vol. 521, no. 7553, p. 460, May 2015.

[32] A. Loquercio, A. I. Maqueda, C. R. del-Blanco, and D. Scaramuzza, "DroNet: Learning to fly by driving," *IEEE Robot. Autom. Lett.*, vol. 3, no. 2, pp. 1088–1095, Apr. 2018.

[33] J. Holis and P. Pechac, "Elevation dependent shadowing model for mobile communications via high altitude platforms in built-up areas," *IEEE Trans. Antennas Propag*, vol. 56, no. 4, pp. 1078–1084, Apr. 2008.

[34] S. Suman, S. Kumar, and S. De, "Path loss model for UAV-assisted RFET," *IEEE Commun. Lett.*, vol. 22, no. 10, pp. 2048–2051, Oct. 2018.

[35] D. P. Bertsekas, *Nonlinear programming*. Athena Scientific Belmont, 1999.

[36] E. W. Weisstein, "Cubic formula," Wolfram MathWorld: A Web Resource, Champaign, IL, USA, 2002. [Online]. Available: http://mathworld.wolfram.com/CubicFormula.html.

[37] Y. Zeng, X. Xu, and R. Zhang, "Trajectory design for completion time minimization in UAV-enabled multicasting," *IEEE Trans. Wireless Commun.*, vol. 17, no. 4, pp. 2233–2246, Apr. 2018.

[38] S. Boyd, L. Xiao, A. Mutapcic, and J. Mattingley, "Notes on decomposition methods," *Notes for EE364B, Stanford University*, pp. 1–36, 2007.

[39] E. L. Lawler, J. K. Lenstra, A. H. G. R. Kan, and D. B. Shmoys, *The traveling salesman problem: a guided tour of combinatorial optimization*. John Wiley & Sons New York, 1985.

[40] D. Mishra, S. De, and K. R. Chowdhury, "Charging time characterization for wireless RF energy transfer," *IEEE Trans. Circuits Syst., II, Exp. Briefs*, vol. 62, no. 4, pp. 362–366, Apr. 2015.

[41] D. Mishra and S. De, "Effects of practical rechargeability constraints on perpetual RF harvesting sensor network operation," *IEEE Access*, vol. 4, pp. 750–765, Mar. 2016.

[42] "Cylinder type Lithium ion capacitors." [Online]. Available: https://www.mouser.com/ds/2/396/capacitor03_e-587718.pdf.

[43] D. Hooper, J. Coughlan, and M. Mullen, "Structural equation modelling: Guidelines for determining model fit," *The Electronic J. Business Research Methods*, vol. 6, pp. 53–60, Jan. 2008.

[44] M. Lu, M. Bagheri, A. P. James, and T. Phung, "Wireless charging techniques for UAVs: A review, reconceptualization, and extension," *IEEE Access*, vol. 6, pp. 29 865–29 884, June 2018.

[45] N. Kingry, L. Towers, Y. Liu, Y. Zu, Y. Wang, B. Staheli, Y. Katagiri, S. Cook, and R. Dai, "Design, modeling and control of a solar-powered quadcopter," in *Proc. IEEE Int. Conf. Robot. Autom. (ICRA)*, Brisbane, QLD, Australia, May 2018, pp. 1251–1258.

[46] Z. F. Pan, L. An, and C. Y. Wen, "Recent advances in fuel cells based propulsion systems for unmanned aerial vehicles," *Applied Ener.*, vol. 240, pp. 473–485, Apr. 2019.

[47] N. K. Ure, G. Chowdhary, T. Toksoz, J. P. How, M. A. Vavrina, and J. Vian, "An automated battery management system to enable persistent missions with multiple aerial vehicles," *IEEE/ASME Trans. Mechatronics*, vol. 20, no. 1, pp. 275–286, Feb. 2015.

[48] T. Pang, K. Peng, F. Lin, and B. M. Chen, "Towards long-endurance flight: Design and implementation of a variable-pitch gasoline-engine quadrotor," in *Proc. IEEE ICCA*, Kathmandu, Nepal, Jun. 2016, pp. 767–772.

Suraj Suman received the B.Tech. degree in Electronics and Communication Engineering from Indian Institute of Information Technology, Design and Manufacturing Jabalpur, India, in 2013, and the M.Tech. degree from Indian Institute of Technology Patna, India, in 2015. He is currently pursuing the Ph.D. degree in the Department of Electrical Engineering at Indian Institute of Technology Delhi, New Delhi, India. His current research interests include green communications, energy harvesting, and aerial communication system.

Sidharth Kumar received the B.Tech. and M.S.(Research) degree in electrical engineering from the Indian Institute of Technology, Delhi, in 2017 and 2019 respectively. His research interests include UAV enabled communication networks, wireless energy transfer, and internet of things (IoT).

Swades De [S'02-M'04-SM'14] received the B.Tech. degree in radiophysics and electronics from the University of Calcutta, Kolkata, India, in 1993, the M.Tech. degree in optoelectronics and optical communication from the Indian Institute of Technology Delhi, New Delhi, India, in 1998, and the Ph.D. degree in electrical engineering from the State University of New York at Buffalo, Buffalo, NY, USA, in 2004.

He is currently a Professor with the Department of Electrical Engineering, IIT Delhi. Before joining IIT Delhi in 2007, he was a tenure-track Assistant Professor with the Department of Electrical and Computer Engineering, New Jersey Institute of Technology, Newark, NJ, USA, from 2004 to 2007. He was an ERCIM Post-Doctoral Researcher with ISTI-CNR, Pisa, Italy, in 2004, and has nearly five years of industry experience in India on communications hardware and software development, from 1993 to 1997, and in 1999. His research interests are in communication networks, with emphasis on performance modeling and analysis.

Dr. De currently serves as a Senior Editor for the IEEE COMMUNICATIONS LETTERS, and an Associate Editor for the IEEE TRANSACTIONS ON VEHICULAR TECHNOLOGY, the IEEE WIRELESS COMMUNICATIONS LETTERS, the IEEE NETWORKING LETTERS, and the IETE Technical Review journal.